Journal of Applied Polymer Science

WILEY

Applied Polymer SCIENCE

RESEARCH ARTICLE

Superhydrophilic and Degradable PLA Fiber Membrane With Silica Layer for Oil-in-Water Emulsion Separation

Li Gao[1,2] | Haihong Gu[2] | Chao Ye[2] | Chunxia Wang[2] | Zimin Jin[1]

[1]College of Textile Science and Engineering, Zhejiang Sci-Tech University, Hangzhou, China | [2]College of Textile and Clothing, Yancheng Institute of Technology, Yancheng, China

Correspondence: Haihong Gu (guhaihong@ycit.edu.cn) | Zimin Jin (jinzimin@zstu.edu.cn)

Received: 9 November 2024 | **Revised:** 8 January 2025 | **Accepted:** 18 February 2025

Funding: This work was supported by the school level research projects of Yancheng Institute of Technology (xjr2021053) and National Natural Science Foundation of China (52303158).

ABSTRACT

A superhydrophilic polylactic acid (PLA) fiber membrane was fabricated by developing a hydrophilic silica surface layer on electrospun fibers. The drawn fibers were twisted and activated in an ethanol solution, leading to the shrinkage of the membrane and enhancing surface hydrophilicity, as well as reducing the pore size of the membrane. Through the coupling of 3-aminopropyltriethoxysilane, silica was polymerized in situ on the fiber surface of the electrospun PLA membrane to achieve a superhydrophilic surface. The membrane underwent degradation in a sodium hydroxide aqueous solution at a rate of 2.240 min^{-1}. The membrane was employed for separating surface-stabilized oil-in-water emulsions. The oil droplet sizes in the filtrates were 93, 169, and 132 nm, respectively. The water flux of the membrane for ionic oil-in-water emulsions reached 3205 $L{\cdot}m^{-2}{\cdot}h^{-1}$, attributed to the electrostatic effect on the membrane surface (35.35 eV) and the sieving effect of the pore channel (0.918 μm). In contrast, the water flux for nonionic emulsions was only 350 $L{\cdot}m^{-2}{\cdot}h^{-1}$. Furthermore, after immersing the membrane in the hydrolysis of tetraethyl orthosilicate again, the oil retention rate remained at 98.6%, and the water flux recovery rate was sustained at 96.3% over 30 cycles of separating oil-in-water emulsion.

1 | Introduction

The production and utilization of equipment in the textile, food, and petrochemical industries result in the inevitable generation of significant volumes of oily wastewater [1–3]. The presence of oil in such wastewater poses challenges for natural degradation, leading to its persistence in the water environment and posing risks to aquatic life, crops, and human health [4–6]. Various treatment approaches for oily wastewater exist, encompassing physical methods like adsorption and membrane separation, chemical techniques such as flocculation and oxidation, and biological processes [7–10]. Among these methods, membrane separation technology is prominent for its efficacy, low energy requirements, and straightforward operation [11–13]. Membrane materials can be fabricated using techniques like biaxial stretching, centrifugal spinning, and electrospinning [14–16]. Electrospun membranes typically feature nanofibers, micron-sized pores, and high porosity [17–19]. Nonetheless, the pore size of electrospun membranes often proves inadequate for addressing water-in-oil emulsions in oily wastewater [20, 21]. Moreover, membranes produced using high molecular weight polymers tend to have hydrophobic surfaces, complicating degradation post disposal [22–24].

The construction of superhydrophilic membrane involves utilizing a hydrophilic surface layer and micro-nano rough structure through surface modification, self-assembly methods, and photoinitiation [25–27]. This membrane allows water to permeate in oil–water separation applications [28–30]. Moreover, the superhydrophilic surface exhibits underwater superoleophobic property, effectively shielding the membrane from oil contamination during the treatment of oily wastewater. The protection

prolongs the membrane's lifespan, enhances material utilization efficiency, and improves oil–water separation performance [31–33]. Incorporating hydrophilic inorganic nanoparticles (e.g., SiO_2, TiO_2, and ZnO) onto the fiber surface of electrospun membranes facilitates the transition from hydrophobicity to hydrophilicity and reduces membrane pore size [34–36]. However, during the oil–water separation process, these nanoparticles may detach from the fiber surface and disperse into the water phase [37, 38]. Additionally, a membrane with a superhydrophilic surface is commonly employed for separating oil–water mixtures and freely dispersed water-in-oil emulsions due to the broad pore size distribution of the membrane [39, 40]. Limited research exists on the separation mechanisms of water-in-oil emulsions stabilized by different surfactants.

In the study, hydrolyzable polylactic acid (PLA) was utilized as the substrate for fabricating fiber membranes through the electrospinning technique. The fibers within the membrane underwent bending upon exposure to ethanol, leading to a reduction in pore distribution. Concurrently, a silica layer was deposited onto the fiber surface via the coupling effect of silane (APTES) to achieve a superhydrophilic surface, thereby minimizing the aggregation of silica particles both within the membrane and on the fiber surface. The mechanical and hydrolytic properties of the PLA fiber membrane were assessed post-treatment with ethanol, APTES, and silica. Subsequently, the separation of surface-stabilized water-in-oil emulsions prepared using anionic (SDBS), cationic (DDBAC), and nonionic (Tween 60) surfactants was investigated employing the superhydrophilic PLA membrane to elucidate the separation mechanism of the emulsions stabilized by different surfactants.

2 | Materials and Methods

2.1 | Materials

PLA (Ingeo 6752D, NatureWorks) was procured from Suzhou Xiayu Plastic Co. Ltd. N,N-dimethylformamide (DMF, AR, 99.5%), ethanol (EtOH, AR, 99.7%), 3-aminopropyltrimethoxysilane (APTES, AR, 99%), tetraethyl orthosilicate (TEOS, GC, 98%), sodium dodecylbenzene sulfonate (SDBS, AR, 98%), and dodecylbenzyldimethylammonium chloride (DDBAC, AR, 99%) were obtained from Shanghai Macklin Biochemical Technology Co. Ltd. Dichloromethane (DCM, AR, 99.5%), Tween 60, and oil red O were sourced from Shanghai Aladdin Biochemical Technology Co. Ltd. Ammonia solution (NH_4OH, AR, 25%) and sodium hydroxide (NaOH, AR, 95%) were purchased from Jiangsu Tongsheng Chemical Reagent Co. Ltd. Deionized water was used for the preparation of all aqueous solutions.

2.2 | Preparation of Superhydrophilic PLA Fiber Membrane

The electrospun PLA fiber membrane was produced using a precursor solution consisting of 9 wt% PLA powder dissolved in a mixture of DCM and DMF (v:v = 7:3). The PLA precursor was electrospun at 11 KV, with a flow rate of 0.01 mL/min and a spinning distance of 15 cm. Electrospinning was conducted at an ambient temperature of 25°C ± 2°C and a relative humidity of 50% ± 5%. Subsequently, a PLA fiber membrane with a thickness of 120 ± 25 μm was obtained. The membrane was then immersed in ethanol for 5 min, followed by a 10-min incubation in a 0.01 M APTES solution composed of ethanol and water (v:v = 1:2). Next, the membrane was transferred to a hydrolysis solution of TEOS, with ammonia serving as a catalyst to expedite the hydrolysis process at 25°C ± 2°C for 30 min. Finally, the membrane was rinsed with water and air-dried. A schematic diagram of the preparation for the superhydrophobic PLA fiber membrane was shown in Figure 1.

2.3 | Characteristic

The fiber morphology and elemental component were examined using a field emission scanning electron microscope (FE-SEM, Nova NanoSEM 450, USA) with an energy dispersive X-ray spectroscopy (EDS). The membrane's apparent roughness (S_q, μm) was determined with a laser confocal microscope (LEXT OLS5000, Japan). The membrane's functional groups were analyzed using infrared spectroscopy (FTIR, NEXUF-670, USA), and its chemical composition was investigated with X-ray photoelectron spectroscopy (XPS, EscaLab 250Xi, China). The contact angle (CA) was measured using a JCY-4 contact angle instrument. The degradation rate of the membrane in 1 M NaOH aqueous solution was expressed by the hydrolysis constant (k, min^{-1}) and measured by the slope of the weight loss over time curve. The surface charge was determined with a solid surface Zeta potential tester (Anton Paar SurPASS, Austria), while mechanical performances were evaluated by a universal mechanical experimenter (ST-500, China). The membrane's pore size distribution and porosity were assessed using a mercury porosimeter (MIP, Autopore 9600, USA). The particle size and electric charge of the oil-in-water emulsion were analyzed using a nanoparticle size and Zeta potential analyzer (Nano ZS90, UK). The oil retention rate (R, %) was calculated using the formula:

$$R = \left(1 - \frac{C_f}{C_0}\right) \times 100$$

where C_f and C_0 represent the oil content in the filtrate and feed emulsions, respectively. The oil content (C, mg/L) was measured with a total organic carbon instrument (TOC, MULTI N-C3100, Germany). The water flux (J, $L \cdot m^{-2} \cdot h^{-1}$) was calculated by measuring the volume of water collected under gravity over a specified period using the formula:

$$R = \frac{V}{A \cdot t}$$

where V (L) is the volume of water collected by the membrane, A is the effective permeation area ($1.767 \times 10^{-4}\ m^2$), and t (h) is the permeation time [41]. The membrane's antifouling capacity was evaluated by determining the flux recovery rate (FRR, %) with the equation:

$$FRR = \frac{J_P}{J_N} \times 100$$

where J_P is the initial water flux in the previous cycle of the oil-in-water emulsion separation process, and J_N is the initial water

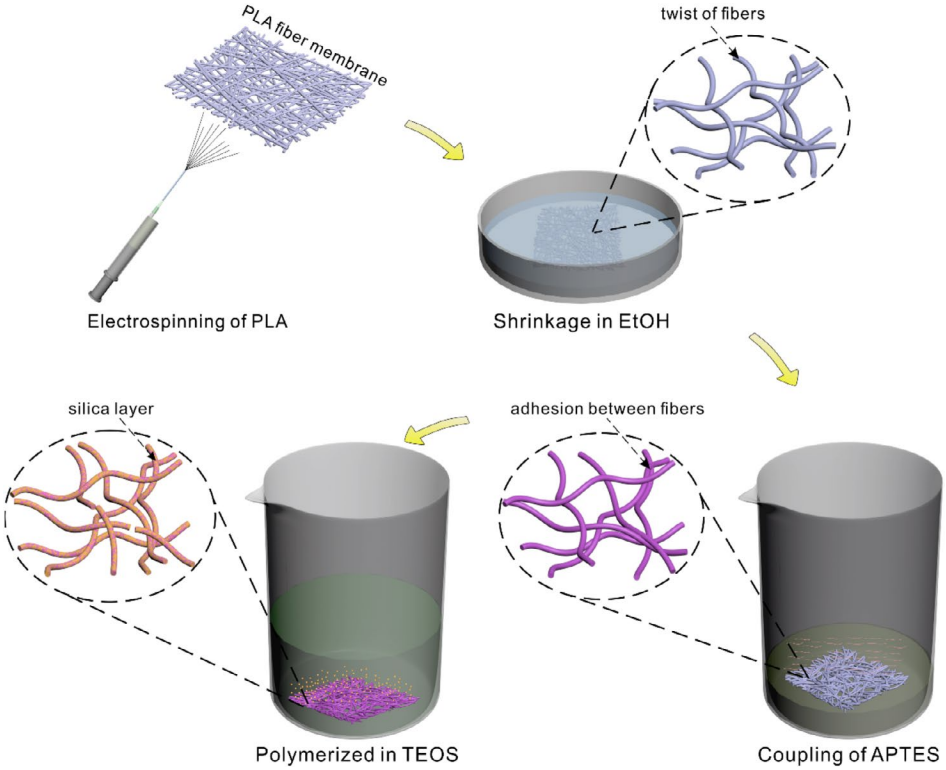

FIGURE 1 | Scheme for the preparation of superhydrophilic PLA fiber membrane. [Color figure can be viewed at wileyonlinelibrary.com]

flux in the next cycle after the membrane was re-immersed in the TEOS hydrolysate [42, 43].

3 | Results and Discussion

3.1 | Morphology and Element of the Membrane

The electrospun PLA membrane exhibited a smooth fiber surface with straight fibers and a diameter distribution ranging from 350 to 980 nm (Figure 2a, Figure S1a and Figure S2a). Upon immersion in ethanol, the fibers bent, causing noticeable planar shrinkage of the membrane at a rate of 80% ± 5% (Figure 2b and Figure S1b). Concurrently, the fiber diameter increased, with the average diameter rising from 622 to 956 nm (Figure S2b). Laser microscopy revealed an increase in membrane roughness post-ethanol immersion, from 3.66 to 4.60 μm (Figure 2eI,II). Infrared spectra displayed characteristic peaks corresponding to various functional groups in the PLA molecular structure, including C═O stretching vibration at 1752 cm^{-1}, C—O—C stretching vibration at 1187 cm^{-1}, and C—H bending vibrations at 1450 and 1380 cm^{-1} (Figure 2fI and Figure S3a) [18]. XPS high-resolution spectra of PLA indicated characteristic peaks of carbon elements, such as C—C/C—H bonds at 285 eV, C—O bonds at 286.5 eV, and O═C—O bonds at 289 eV (Figure 3a) [25]. Ethanol treatment of the membrane revealed a bending vibration of —OH at 1644 cm^{-1} in the FTIR spectra (Figure 2fII and Figure S3b). Despite an increase in oxygen content (from 29.7% to 33.6%, Table S1a,b), no new elements were detected in the XPS spectra (Figure S4a,b). Comparison of the electrospun PLA membrane with the ethanol-treated membrane in the high-resolution XPS spectra of O1s showed the persistence of the characteristic peak corresponding to O═C—O at 532 eV, alongside a higher intensity of the characteristic peak corresponding to —OH at 533.5 eV (Figure 3b and Figure S5a) [29].

Upon APTES treatment of the PLA membrane, enhanced adhesion between fibers was observed (Figure 2c and Figure S1c), while the fiber diameter remained unchanged (Figure S2c). The roughness of the membrane was minimally affected by the APTES treatment (Figure 2eIII). FTIR spectra revealed characteristic peaks of N—H bending vibration at 1568 cm^{-1} and Si—C stretching vibration at 697 cm^{-1} (Figure 2fIII), with the presence of Si and N elements confirmed in the XPS spectra (Figure S4c and Table S1c) [13]. High-resolution XPS spectra of N1s displayed nitrogen peaks at 399.46 eV (representing the N—C bond) and at 401.34 eV (representing the $—NH_2$ group) (Figure 3c) [38]. Additionally, a characteristic peak corresponding to Si—O—C at 102 eV was observed (Figure S5b), indicating the encapsulation of APTES on the fiber surface of the membrane [44].

When the APTES-treated membrane was placed in the hydrolysis solution of TEOS, a decrease in fiber adhesion was observed, accompanied by fiber breakage (Figure 2d and Figure S1d). Furthermore, the average fiber diameter increased to 1100 nm (Figure S2d), while the membrane roughness was enhanced to 5.49 μm (Figure 2eIV). The FTIR spectra revealed a stretching vibration peak of Si—O—Si at 796 cm^{-1} (Figure 2fIV) [41]. Additionally, high-resolution XPS spectra of Si2p exhibited distinct characteristic peaks at 104.59 and 100.87 eV, corresponding to Si—O—Si and SiC bonds, respectively (Figure 3d) [21].

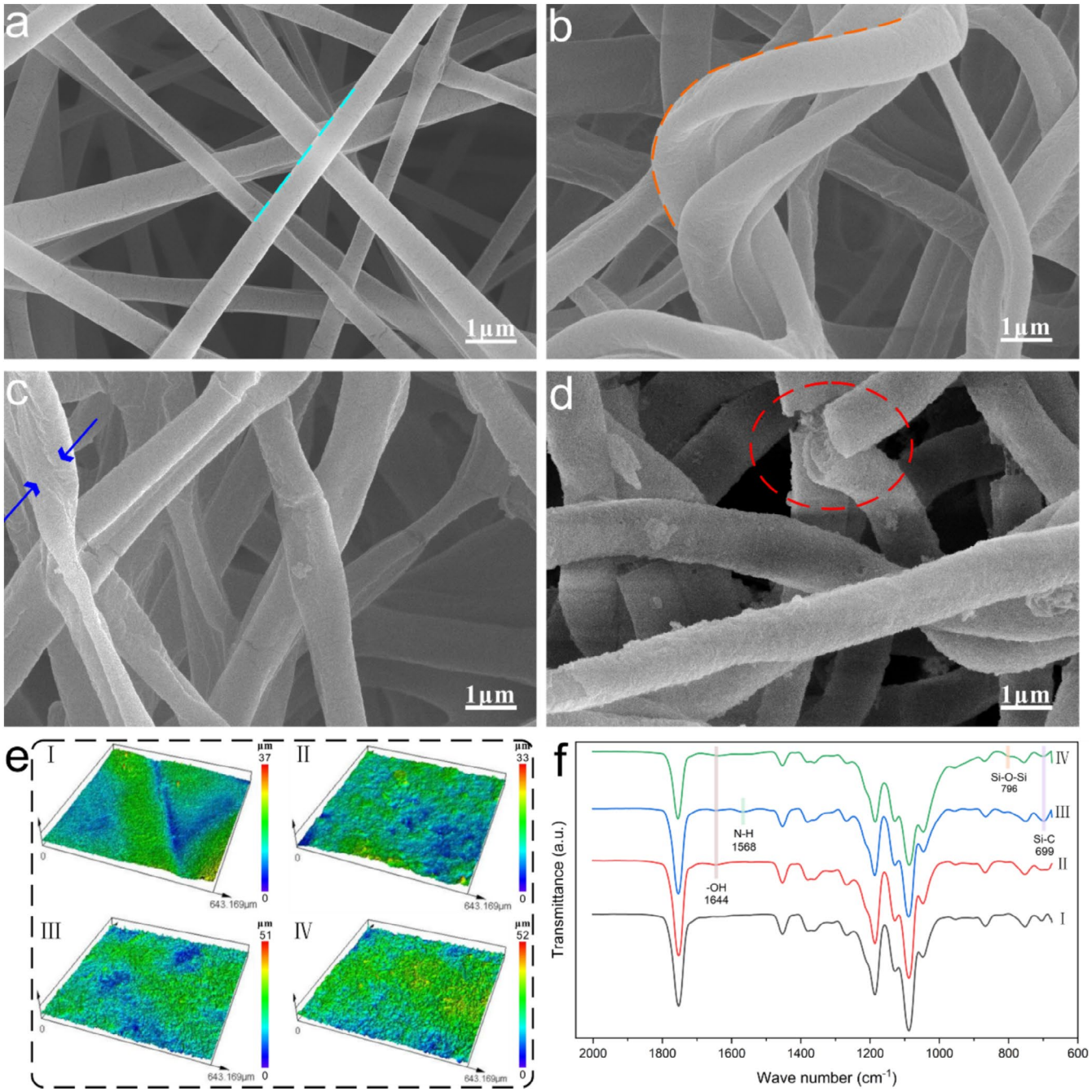

FIGURE 2 | (a–d) SEM images, (e) laser microscope images, and (f) FTIR spectra of the PLA fiber membranes with the different treatments: (I) electrospun, (II) soaked in EtOH, (III) treated with APTES, and (IV) placed in the hydrolysis solution of TEOS. [Color figure can be viewed at wileyonlinelibrary.com]

3.2 | Surface Wettability of the Membrane

The hydrophilicity of the membrane was assessed using the water contact angle (WCA). The electrospun PLA fiber membrane exhibited hydrophobic properties, as indicated by a WCA of 126.7°, which remained stable over time (10 min, Figure 4aI). The membrane dissolved in dichloromethane (DCM) when submerged in water (Figure 4bI). Following immersion in ethanol, the initial WCA of the membrane was 109.5°. Within 60 s, the water droplet infiltrated the membrane, resulting in a final WCA of 42.5° (Figure 4aII). The membrane continued to exhibit high permeability to DCM in water (Figure 4bII). Treatment with APTES further enhanced the membrane's hydrophilicity, enabling water droplet penetration within 1.2 s (Figure 4aIII). However, the membrane displayed lipophilic behavior underwater, allowing DCM to spread around its surface in water (Figure 4bIII). In situ polymerization of silica during TEOS hydrolysis on the fiber surface resulted in a super hydrophilic membrane (SiO_2/PLA membrane) with water droplet penetration occurring within 0.15 s (Figure 4aIV). Additionally, the membrane exhibited underwater superoleophobic properties, with the underwater oil contact angle (UOCA) significantly increasing to 153.2°. DCM on the membrane maintained a subcircular shape in water (Figure 4bIV). Importantly, the SiO_2/PLA

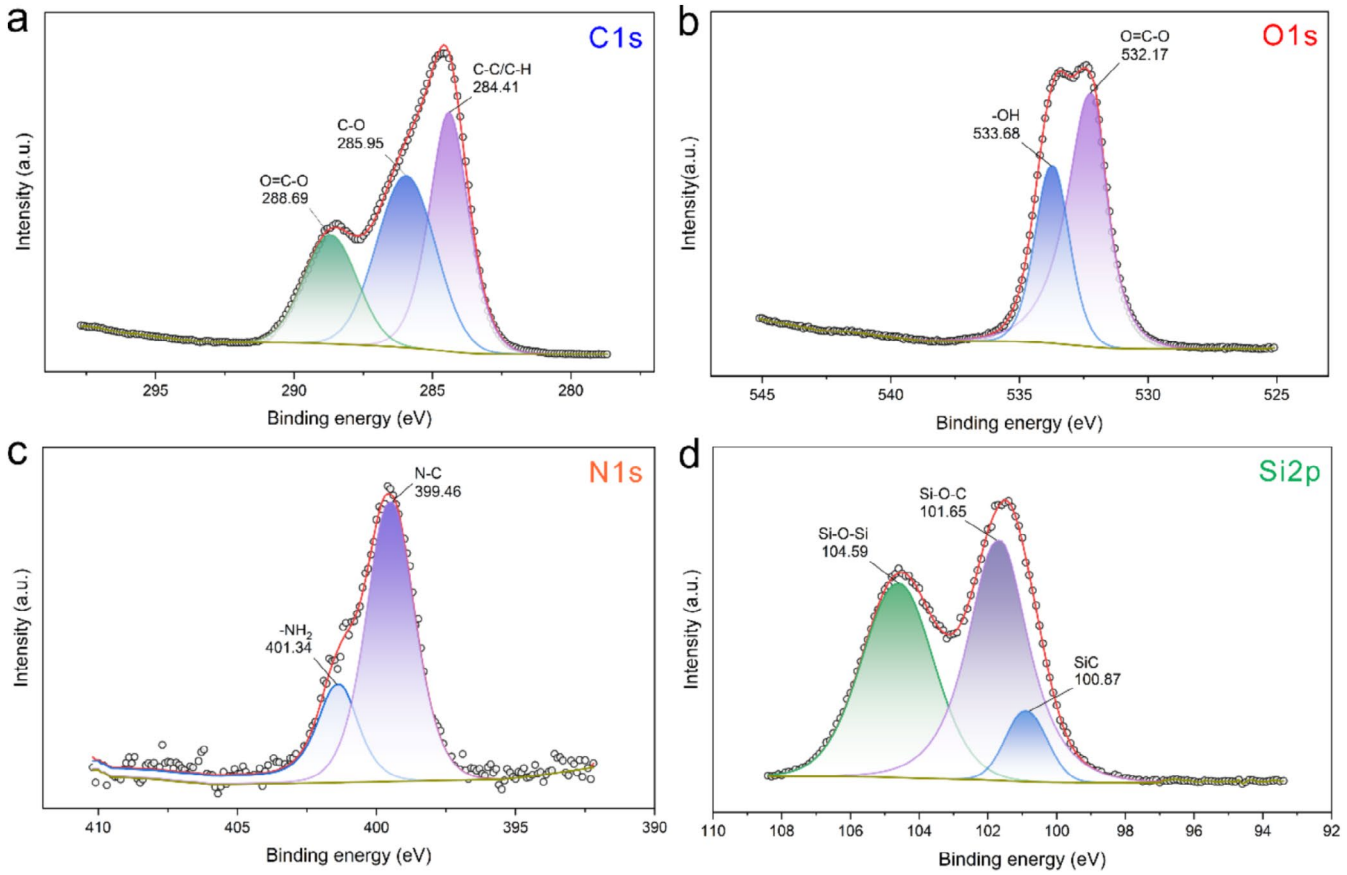

FIGURE 3 | High-resolution XPS spectra of the PLA fiber membranes with the different treatments: (a) electrospun, (b) soaked in EtOH, (c) treated with APTES, and (d) placed in the hydrolysis solution of TEOS. [Color figure can be viewed at wileyonlinelibrary.com]

membrane was not dissolved by DCM due to the silica forming a protective layer on the fiber surface, effectively preventing contact between DCM and the membrane.

The degradation rate of the membrane in NaOH aqueous solution was depicted in Figure 4c. After immersion in ethanol, PLA underwent swelling, resulting in an increase in fiber diameter. This swelling weakened the interaction between PLA chains, leading to an expansion in the distance between molecular chains [45]. Consequently, there was an enhanced pathway for water molecules to permeate the PLA structure. The hydrophilicity of the PLA surface was heightened post-ethanol treatment, facilitating the adsorption and diffusion of water molecules on the PLA surface. These accelerated the degradation process of PLA by increasing the reaction rate between PLA and water. The degradation rate of the membrane increased from 0.683 to 2.855 min^{-1} after ethanol immersion (Figure 4cI,II). When the PLA membrane was treated with APTES, the surface hydrophilicity significantly improved, making it more conducive for water molecules to adhere and spread across the surface. Additionally, the introduction of an amino group (—NH_2) via APTES coupling enhanced the degradation of PLA by elevating the local pH through proton transfer reactions in alkaline conditions. The degradation rate of the APTES-treated membrane obviously increased to 8.540 min^{-1} (Figure 4cIII). The inherent hydrophilicity of the SiO_2 cladding amplified the interfacial interaction between PLA and water. The SiO_2 surface possessed the propensity to attract water molecules, thereby fostering the retention and diffusion of water molecules on the PLA surface and expediting the degradation reaction. In contrast, the degradation rate of the SiO_2-treated membrane remained at 2.240 min^{-1} (Figure 4cIV).

The surface potential analysis revealed that the electrospun PLA membrane surface was negatively charged (−45.74 eV, Figure 4dI) in water (pH = 7). Post-ethanol immersion, the negative charge intensified (−53.79 eV, Figure 4dII) due to hydroxyl group (—OH) formation on the membrane surface. APTES treatment induced a shift to a positive surface charge (42.07 eV, Figure 4dIII) in water, likely due to the presence of the —NH_2 group in the APTES chain segment. Silica polymerization on the fiber surface slightly reduced the positive charge (35.35 eV, Figure 4dIV) attributed to the —OH group on the hydrophilic silica surface formed by TEOS hydrolysis and condensation.

Figure 4e illustrated the mechanical properties of PLA membranes, demonstrating an elongation at break of 44.1% and a breaking strength of 2.395 MPa for the electrospun PLA fiber membrane (Figure 4eI). Upon immersion in alcohol, the twisted and tangled fiber segments required straightening before breaking, thereby increasing the elongation at break to 50.1%. However, the twisting and tangling of fibers restricted the sliding between them, reducing their ability to disperse stresses through relative sliding during stretching [46]. This restriction results in a more pronounced local stress concentration in the twisted and tangled regions, leading to a decrease in fracture strength to

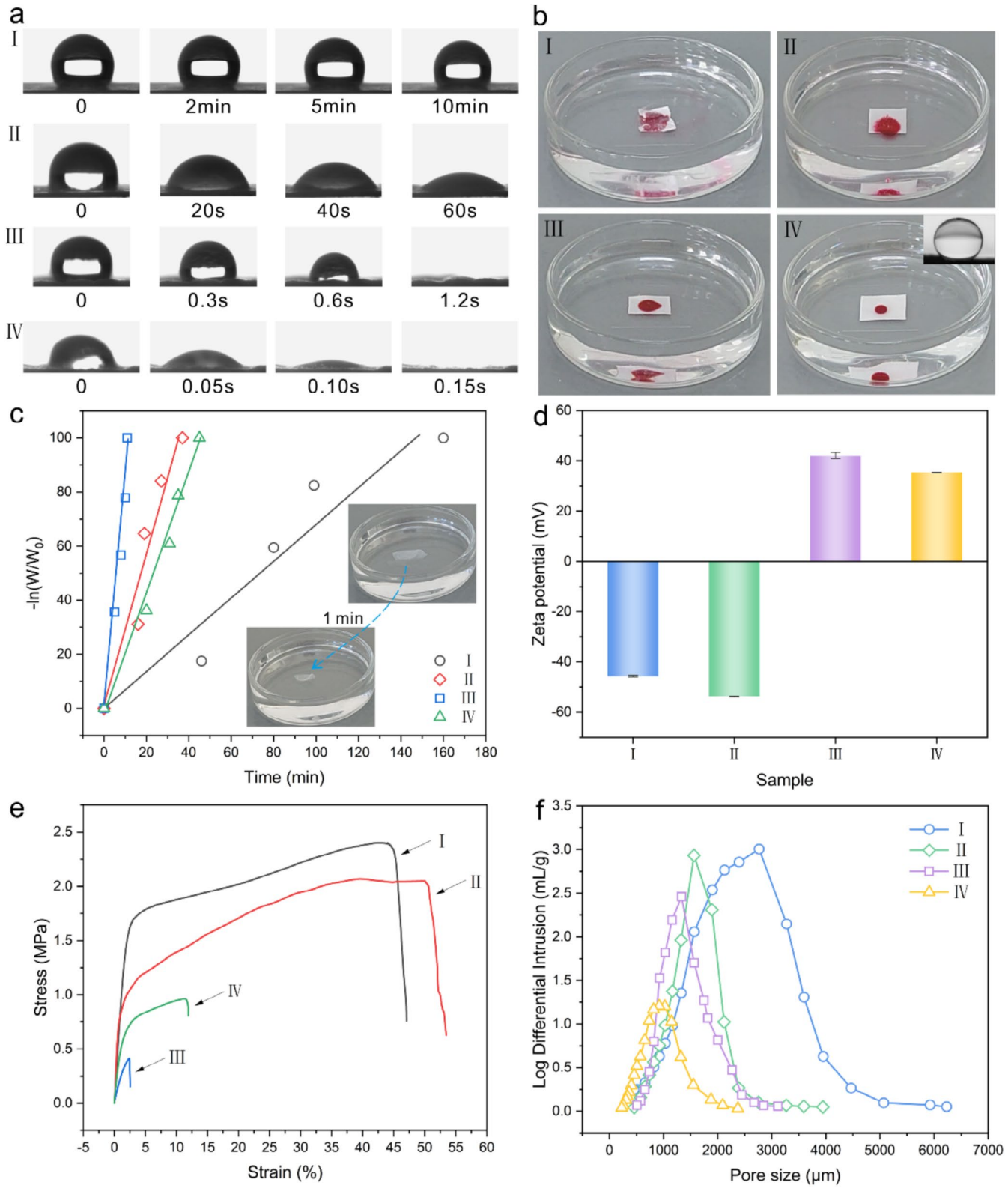

FIGURE 4 | (a) Water contact angle, (b) state of DCM droplet on the membrane surface underwater, (c) weight loss-time curve in NaOH aqueous solution, (d) solid surface charge, (e) stress–strain curve, (f) pore size distribution of the membranes with the different treatments: (I) electrospun, (II) soaked in EtOH, (III) treated with APTES, and (IV) placed in the hydrolysis solution of TEOS. [Color figure can be viewed at wileyonlinelibrary.com]

2.045 MPa (Figure 4eII). Treatment with the APTES enhanced the adhesion between fibers, limiting their sliding and independent deformation ability [47]. Consequently, the membrane lost its original flexibility, becoming stiff and experiencing a significant decrease in fracture strength (0.406 MPa) and elongation at break (2.4%) (Figure 4eIII). The silica coating diminished the adhesion between fibers, enabling freer sliding and deformation during stretching, thereby improving the independent

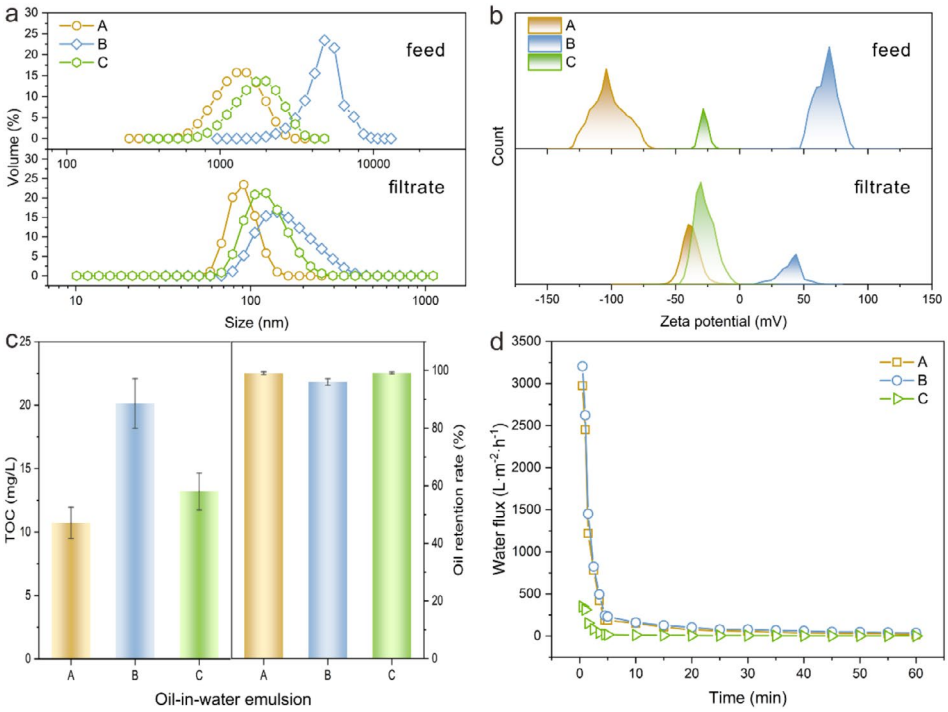

FIGURE 5 | (a) Oil droplet size, (b) Zeta potential, (c) TOC and oil retention rate, and (d) water flux of the membrane separation for the oil-in-water emulsions prepared with different surfactants: (A) anionic surfactant (SDBS), (B) cationic surfactant (DDBAC) and (C) nonionic surfactant (Tween 60). [Color figure can be viewed at wileyonlinelibrary.com]

strain between fibers to 11.6%. Although some fibers fractured post-silica coating, these fractures occurred independently rather than due to adhesion or stress concentrations, resulting in an increased breaking strength to 0.963 MPa (Figure 4eIV). Conversely, fibers with adhesion tendencies exhibited localized stress concentrations during stretching, leading to premature brittle fracture.

The pore structure was analyzed as illustrated in Figure 4f. The electrospun PLA fiber membrane exhibited a relatively large pore size, with an average of 2.765 μm (Figure 4fI) and a porosity of 70.39% (Figure S6). Emulsified oil containing particles of 1 μm could infiltrate the membrane pores, hindering effective oil–water separation. Subsequent immersion in ethanol led to a significant reduction in pore size and porosity to 1.564 μm and 54.64%, respectively, due to membrane shrinkage (Figure 4fII). Treatment with APTES further decreased the pore size and porosity to 1.332 μm and 48.18% (Figure 4fIII) by enhancing fiber adhesion. In situ polymerization of silica on the fiber surface resulted in an average pore size of 0.918 μm and a porosity of 43.91% (Figure 4fIV), offering potential for emulsified oil physical screening.

3.3 | Oil-in-Water Emulsion Separation

The SiO_2/PLA membrane exhibited nanoscale pore size and superhydrophilic surface, undergoing planar shrinkage and in situ surface polymerization of hydrophilic silica, enabling the separation of oil-in-water emulsions. Three surface-stabilized oil-in-water emulsions were created using SDBS (anionic surfactant), DDBAC (cationic surfactant), and Tween 60 (nonionic surfactant). The emulsions were separated by the SiO_2/PLA membrane under gravity. The average particle sizes of the oil droplets in the emulsions prepared with the three surfactants were 1374, 4685, and 1838 nm, respectively. Post-membrane separation, the droplet sizes in the filtrate notably decreased to 93, 169, and 132 nm, as depicted in Figure 5a. Furthermore, the zeta potential of the emulsion prepared with SDBS was −104 mV, increasing to −40 mV in the filtrate after separation. For the emulsion prepared with DDBAC, the zeta potential was 70 mV, decreasing to 44 mV in the filtrate. The emulsion prepared with Tween 60 had a zeta potential of −25 mV, with minimal change in the filtrate, as shown in Figure 5b. Additionally, the oil contents in the emulsions prepared with SDBS, DDBAC, and Tween 60 were assessed using total organic carbon (TOC). Following membrane separation, the TOC in the filtrates decreased to 11, 20, and 13 mg/L, respectively, and the oil retention rates of the emulsions were 99.1%, 96.0%, and 99.3%, respectively (Figure 5c). Furthermore, the water flux of the membrane separation for the oil-in-water emulsion was depicted in Figure 5d. Initially, the water fluxes for membrane separation of oil-in-water emulsions prepared with SDBS, DDBAC, and Tween 60 were 2973, 3205, and 350 $L \cdot m^{-2} \cdot h^{-1}$, respectively. Subsequently, the water fluxes of the membranes exhibited a significant decrease over time, stabilizing at a lower level during the separation process of oil-in-water emulsions under gravity.

The stability of membrane separation for oil-in-water emulsions, as illustrated in Figure 6a, revealed a consistent oil retention rate exceeding 98.6% over 30 separation cycles for emulsions prepared with SDBS. However, an increase in the number of separations caused a decline in water flux due to the depletion of charge on the silica layer of the fiber surface and the accumulation of an oil layer on the membrane surface (Figure S7). To address this, the membrane was re-immersed in TEOS hydrolysate

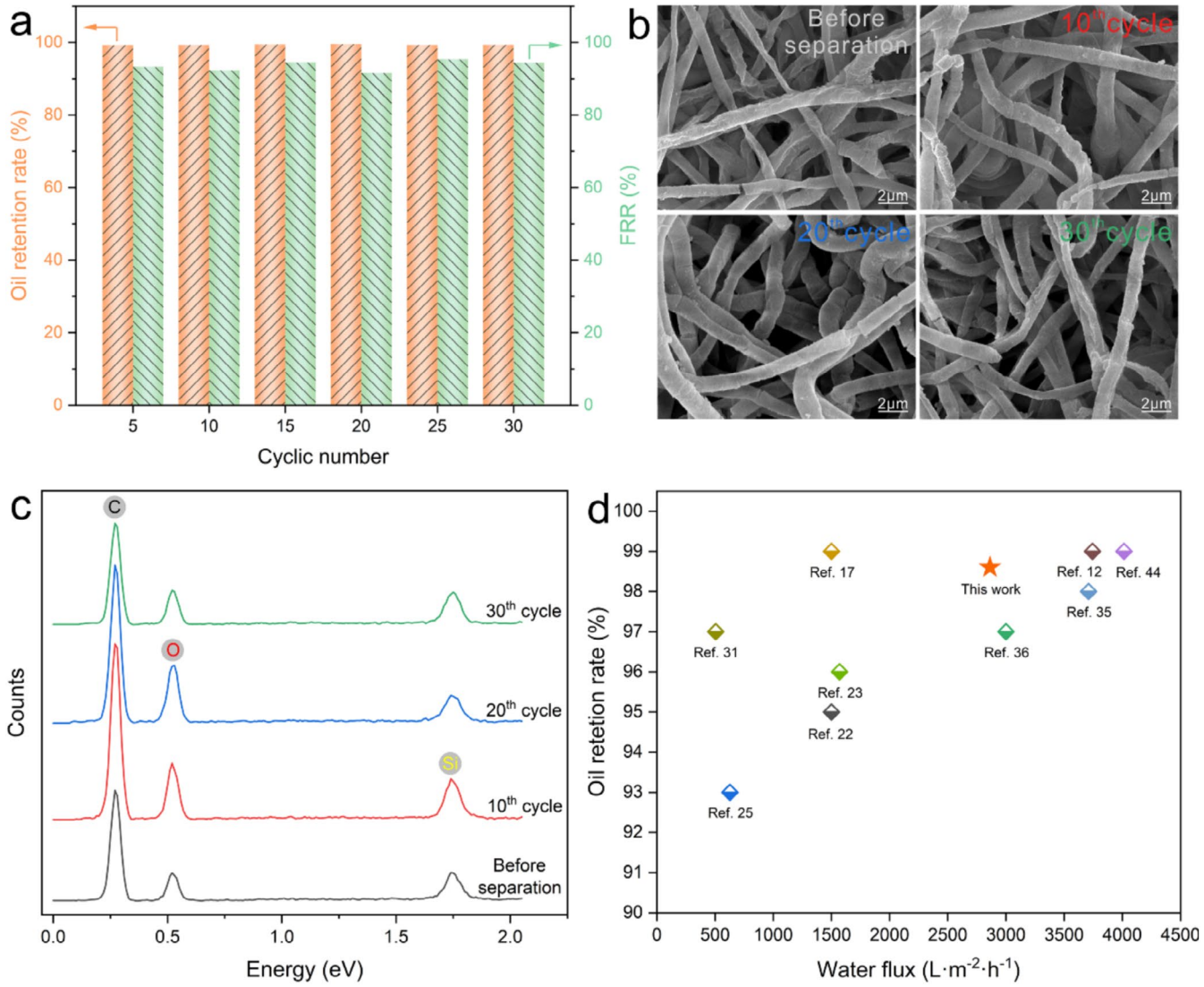

FIGURE 6 | (a) Oil retention rate and water flux recovery rate (FRR), (b) SEM images, (c) EDS analysis of the membrane for the oil-in-water emulsion prepared with SDBS during the cyclic separation, and (d) comparison of the separation performance for oil-in-water emulsion by the membrane prepared in this work with other hydrophilic electrospun membranes reported in the literature. [Color figure can be viewed at wileyonlinelibrary.com]

post-separation to regenerate the original silica layer on the fiber surface, resulting in a water flux recovery rate of 96.3% during cyclic separation of oil-in-water emulsions prepared with SDBS. The morphology and chemical analysis of the membrane after cyclic separation were depicted in Figure 6b,c, revealing that the fibers of the membrane retained the twisted morphology with the silica layer covering the surface. The membrane maintained its porous structure without any signs of blockage. EDS analysis indicated that the chemical composition of the membrane remained unchanged, with predominant elements being C, O, and Si, suggesting stability in micro-morphology and chemical composition. In comparison to other hydrophilic electrospun membranes in the literature, the SiO_2/PLA membrane exhibited superior performance in cyclic separation of oil-in-water emulsion, demonstrating high water flux and oil retention rate, as illustrated in Figure 6d.

Ionic surfactants lead to the formation of micelles on the surface of oil droplets, ensuring their stable dispersion in water [48]. The emulsified interface created by ionic surfactants carried a negative or positive charge [49]. Upon contact with the membrane surface bearing a positive charge in water, the stability of the emulsified interface of the oil droplets was disrupted due to physical pore squeezing (Figure 7a) and electrostatic effects (Figure 7b,c) on the fiber surface [50, 51]. Consequently, the oil droplets were released from the micelles, rose due to buoyancy, and coalesced into larger oil droplets [52], as depicted in Figure 7d. The electrostatic interaction (including electrostatic adsorption and repulsion) between the membrane surface and the emulsified interface diminished the surface charge of the oil droplets in the filtrate, causing the zeta potential of the filtrate to approach that of water [53]. In emulsions prepared with cationic surfactants, the larger size of the oil droplets and less stable emulsified interface made them more susceptible to destruction during membrane separation [54]. Hence, the water flux of the oil-in-water emulsion prepared with DDBAC surpassed that of the emulsion prepared with SDBS. Conversely, the emulsified interface formed

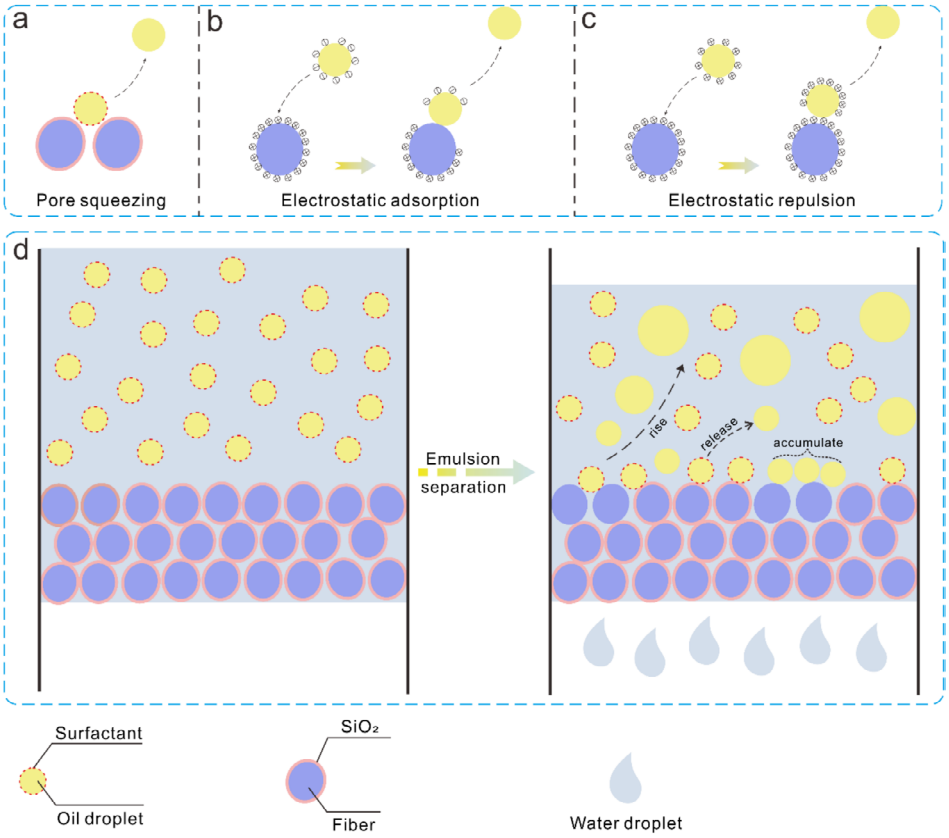

FIGURE 7 | Separation mechanism of the superhydrophilic PLA fiber membrane for the oil-in-water emulsion. [Color figure can be viewed at wileyonlinelibrary.com]

by nonionic surfactants lacked charge distribution, leading to minimal zeta potential variation before and after separation, aligning closely with the zeta potential of water [55]. During membrane separation, the sieving effect (physical squeezing) of the pore channels only existed to disrupt the emulsified interface of oil droplets in water-in-oil emulsions prepared with Tween 60, resulting in low water flux [56]. As separation progressed, oil droplets accumulated on the membrane surface, forming an oil layer that hindered water passage through the membrane pores, leading to a sustained reduction in water flux [57].

4 | Conclusion

PLA fiber membrane was fabricated via electrospinning, exhibiting an average diameter of 622 nm and a pore size of 2.765 μm. The electrospinning process imparted straightness to the fibers within the membrane. Subsequent immersion of the membrane in ethanol induced fiber twisting and membrane shrinkage, leading to a reduction in pore size to 1.564 μm. Furthermore, the hydrophilicity of the membrane was enhanced by the introduction of a hydroxyl group (—OH) from the ethanol. Treatment of the membrane with APTES facilitated fiber adhesion. The coupling of APTES prompted the formation of a silica layer on the fiber surface through the hydrolysis of TEOS, resulting in the creation of a superhydrophilic surface with underwater superoleophobicity (UOCA:153.2°). This surface modification served to protect against the diffusion and dissolution of DCM on the membrane surface. The hydrophilicity of SiO_2 facilitated water molecule retention and diffusion on the PLA surface, accelerating the degradation reaction. The degradation rate of the SiO_2-treated membrane remained constant at 2.240 min^{-1}. Additionally, the silica coating decreased interfiber adhesion by coupling with APTES, enhancing membrane strain to 11.6% and breaking strength to 0.963 MPa.

The superhydrophilic PLA membrane with a pore size of 0.918 μm was utilized to separate surface-stabilized oil-in-water emulsions containing SDBS, DDBAC, and Tween 60. The oil droplet sizes in the filtrates measured 93, 169, and 132 nm, respectively, with corresponding total organic carbon (TOC) contents of 11, 20, and 13 g/mL. The membrane's positive charge (35.35 eV) facilitated the separation of ionic emulsions through electrostatic interactions with the oil droplets' emulsified interfaces. Water flux of the membrane for emulsions prepared with SDBS and DDBAC reached 2973 and 3205 $L \cdot m^{-2} \cdot h^{-1}$, respectively, while the flux for the emulsion containing Tween 60 was lower at 350 $L \cdot m^{-2} \cdot h^{-1}$, primarily due to the sieving effect of the pore channel alone. Water flux decreased over time as oil droplets accumulated on the membrane surface, forming an oil layer. Moreover, water flux decreased with the number of separation cycles. When the separated membrane was immersed in the hydrolysis of TEOS again, the membrane exhibited a water flux recovery rate of 96.3% after 30 cycles of separating oil-in-water emulsions prepared with SDBS. Throughout the cyclic separation process,

the membrane maintained an oil retention rate of 98.6% for the emulsion.

Author Contributions

Li Gao: writing – original draft (equal). **Haihong Gu:** writing – review and editing (lead). **Chao Ye:** funding acquisition (supporting). **Chunxia Wang:** investigation (equal). **Zimin Jin:** methodology (equal).

Acknowledgments

This work received support from the school-level research projects of Yancheng Institute of Technology (xjr2021053) and the National Natural Science Foundation of China (52303158).

Conflicts of Interest

The authors declare no conflicts of interest.

Data Availability Statement

The data that support the findings of this study are available from the corresponding author upon reasonable request.

References

1. R. Sarbatly and C. K. Chiam, "An Overview of Recent Progress in Nanofiber Membranes for Oily Wastewater Treatment," *Nanomaterials* 12 (2022): 2919–2937, https://doi.org/10.3390/nano12172919.

2. F. Yalcinkaya, E. Boyraz, J. Maryska, and K. Kucerova, "A Review on Membrane Technology and Chemical Surface Modification for the Oily Wastewater Treatment," *Materials* 13, no. 2 (2020): 493–506, https://doi.org/10.3390/ma13020493.

3. J. L. Gong, B. Xiang, Y. Q. Sun, and J. Li, "Janus Smart Materials With Asymmetrical Wettability for On-Demand Oil/Water Separation: A Comprehensive Review," *Journal of Materials Chemistry A* 11 (2023): 25093–25114, https://doi.org/10.1039/d3ta04160c.

4. C. J. Singh, S. Mukhopadhyay, and R. S. Rengasamy, "Fibrous Coalescence Filtration in Treating Oily Wastewater: A Review," *Journal of Industrial Textiles* 51 (2021): 3648S–3682S, https://doi.org/10.1177/15280837211040863.

5. M. G. Barron, D. N. Vivian, R. A. Heintz, and U. H. Yim, "Long-Term Ecological Impacts From Oil Spills: Comparison of Exxon Valdez, Hebei Spirit and Deepwater Horizon," *Environmental Science & Technology* 54 (2020): 6456–6467, https://doi.org/10.1021/acs.est.9b05020.

6. Y. Y. Peng, Y. Liu, J. Y. Dai, et al., "A Sustainable Strategy for Remediation of Oily Sewage: Clean and Safe," *Separation and Purification Technology* 240 (2020): 116592–116601, https://doi.org/10.1016/j.seppur.2020.116592.

7. H. J. Lu, Y. H. Zhang, B. Zhang, et al., "Preparation of Newly Polymer-Coated Microbial Pellets and Their Adsorption and Degradation Properties for Oil-Containing Wastewater," *Langmuir* 40 (2024): 11239–11250, https://doi.org/10.1021/acs.langmuir.4c00994.

8. A. Bhattacharyya, L. Liu, K. Lee, and J. Miao, "Review of Biological Processes in a Membrane Bioreactor (MBR): Effects of Wastewater Characteristics and Operational Parameters on Biodegradation Efficiency When Treating Industrial Oily Wastewater," *Journal of Marine Science and Engineering* 10, no. 9 (2022): 1229–1245, https://doi.org/10.3390/jmse10091229.

9. C. L. Zhao, J. Y. Zhou, Y. Yan, et al., "Application of Coagulation/Flocculation in Oily Wastewater Treatment: A Review," *Science of the Total Environment* 765 (2021): 142795–142811, https://doi.org/10.1016/j.scitotenv.2020.142795.

10. K. Du, M. He, M. L. Lian, et al., "Catalytic Wet Air Oxidation Treatment of Oily Wastewaters," *Chemistry and Technology of Fuels and Oils* 52 (2016): 85–89, https://doi.org/10.1007/s10553-016-0676-3.

11. F. Abuhantash, H. M. Hegab, I. H. Aljundi, and S. W. Hasan, "Synergistic Design of Polylactic Acid/Functionalized Multi-Walled Carbon Nanotubes Composite Membrane for Enhanced Oil-Water Separation," *Journal of Environmental Chemical Engineering* 11, no. 6 (2023): 111566–111577, https://doi.org/10.1016/j.jece.2023.111566.

12. J. Lu, J. X. Wen, Q. H. Yu, C. Cui, J. Su, and J. Han, "Cellulose Nanospheres Coated Polylactic Acid Nonwoven Membranes for Recyclable Use in Oil/Water Separation," *Cellulose* 28 (2021): 11417–11427, https://doi.org/10.1007/s10570-021-04247-1.

13. B. R. Ye, C. Jia, Z. W. Li, et al., "Solution-Blow Spun PLA/SiO_2 Nanofiber Membranes Toward High Efficiency Oil/Water Separation," *Journal of Applied Polymer Science* 137, no. 37 (2020): 49103–49111, https://doi.org/10.1002/app.49103.

14. X. H. Li, S. L. Zhang, J. Z. Li, et al., "Bio-Degradable Fibrous Membranes for Oil/Water Separation by Melt Electrospinning," *Journal of Applied Polymer Science* 141, no. 39 (2024): 56018–56031, https://doi.org/10.1002/app.56018.

15. X. T. Yu, X. Zhang, H. J. Zhang, et al., "Preparation of a Janus-Polyvinylidene Fluoride Micro/Nano Fiber Membrane by Centrifugal Spinning and Investigation Into Its Unidirectional Water Transfer and Oil-Water Separation Functions," *Textile Research Journal* 93 (2023): 2894–2907, https://doi.org/10.1177/00405175221148265.

16. C. X. Wan, T. Cao, X. Chen, L. Meng, and L. Li, "Fabrication of Polyethylene Nanofibrous Membranes by Biaxial Stretching," *Materials Today Communications* 17 (2018): 24–30, https://doi.org/10.1016/j.mtcomm.2018.08.004.

17. C. M. Jiang, M. Hua, G. X. Mu, et al., "Superhydrophilic and Underwater Superoleophobic Polylactide/Cellulose Diacetate Composite Nanofibrous Membranes for Effective Oil-In-Water Emulsions Separation," *Separation and Purification Technology* 348 (2024): 127806–127819, https://doi.org/10.1016/j.seppur.2024.127806.

18. Y. H. Yu, W. L. Li, W. T. Lin, P. Fu, Z. K. Xu, and L. S. Wan, "High Permeance Polyamide Nanofiltration Membranes Based on Poly(L-Lactic Acid) Electrospun Nanofibrous Membranes With Controlled Hydrophilicity," *ACS Applied Nano Materials* 7 (2024): 12003–12014, https://doi.org/10.1021/acsanm.4c01635.

19. C. M. Jiang, Y. Tian, L. L. Wang, et al., "Facile Approach for the Potential Large-Scale Production of Polylactide Nanofiber Membranes With Enhanced Hydrophilic Properties," *Materials* 16, no. 5 (2023): 1784–1794, https://doi.org/10.3390/ma16051784.

20. J. Y. Zhang, F. Zhang, W. X. Fang, J. Zhang, W. Fang, and J. Jin, "Membrane Wettability Manipulation via Mixed-Dimensional Heterostructured Surface Towards Highly Efficient Oil-in-Water Emulsion Separation," *Journal of Membrane Science* 672 (2023): 121472–121480, https://doi.org/10.1016/j.memsci.2023.121472.

21. B. S. Shen, C. X. Du, W. Wang, et al., "Hydrophilic SPE/MPTES-PAN Electrospun Membrane Prepared via Click Chemistry for High Efficiency Oil-Water Separation," *Journal of Materials Science* 57 (2022): 1474–1488, https://doi.org/10.1007/s10853-021-06688-2.

22. H. D. Zhao, Y. L. He, Z. H. Wang, et al., "Mussel-Inspired Fabrication of PDA@PAN Electrospun Nanofibrous Membrane for Oil-in-Water Emulsion Separation," *Nanomaterials* 11, no. 12 (2021): 3434–3448, https://doi.org/10.3390/nano11123434.

23. H. N. Doan, P. P. Vo, A. Baggio, et al., "Environmentally Friendly Chitosan-Modified Polycaprolactone Nanofiber/Nanonet Membrane for Controllable Oil/Water Separation," *ACS Applied Polymer Materials* 3 (2021): 3891–3901, https://doi.org/10.1021/acsapm.1c00463.

24. H. Yin, J. Zhao, Y. Q. Li, et al., "A Novel Pd Decorated Polydopamine-SiO_2/PVA Electrospun Nanofiber Membrane for Highly Efficient Degradation of Organic Dyes and Removal of Organic Chemicals and Oils," *Journal of Cleaner Production* 275 (2020): 122937–122946, https://doi.org/10.1016/j.jclepro.2020.122937.

25. D. C. Zhong, X. Y. Wang, and J. J. Wang, "Green Electrospun Poly(Vinyl Alcohol)/silicon Dioxide Nanofibrous Membrane Coated With Polydopamine in the Presence of Strong Oxidant for Effective Separation of Surfactant-Stabilized Oil-in-Water Emulsion," *Surface and Coatings Technology* 460 (2023): 129421–129431, https://doi.org/10.1016/j.surfcoat.2023.129421.

26. Y. J. Ding, J. D. Wu, J. Q. Wang, et al., "Superhydrophilic and Mechanical Robust PVDF Nanofibrous Membrane Through Facile Interfacial Span 80 Welding for Excellent Oil/Water Separation," *Applied Surface Science* 485 (2019): 179–187, https://doi.org/10.1016/j.apsusc.2019.04.214.

27. L. L. Gong, L. Zhang, N. X. Wang, et al., "In Situ Ultraviolet-Light-Induced TiO_2 Nanohybrid Superhydrophilic Membrane for Pervaporation Dehydration," *Separation and Purification Technology* 122 (2014): 32–40, https://doi.org/10.1016/j.seppur.2013.10.032.

28. X. Ma, C. Y. Wang, H. X. Guo, et al., "Novel Dopamine-Modified Cellulose Acetate Ultrafiltration Membranes With Improved Separation and Antifouling Performances," *Journal of Materials Science* 57 (2022): 6474–6486, https://doi.org/10.1007/s10853-022-07024-y.

29. Z. Xiong, H. B. Lin, Y. Zhong, et al., "Robust Superhydrophilic Polylactide (PLA) Membranes With a TiO_2 Nano-Particle Inlaid Surface for Oil/Water Separation," *Journal of Materials Chemistry A* 5, no. 14 (2017): 6538–6545, https://doi.org/10.1039/c6ta11156d.

30. B. Xiang, J. Gong, Y. Sun, W. Yan, R. Jin, and J. Li, "High Permeability PEG/MXene@MOF Membrane With Stable Interlayer Spacing and Efficient Fouling Resistance for Continuous Oily Wastewater Purification," *Journal of Membrane Science* 691 (2024): 122247–122261, https://doi.org/10.1016/j.memsci.2023.122247.

31. S. M. Moatmed, M. H. Khedr, S. I. El-Dek, et al., "Multifunctional Nanofiber Membrane for High Removal Efficiency of Biological/Organic Contaminations and Oil-In-Water Emulsion Under Gravity-Driven Separation," *Journal of Molecular Liquids* 394 (2024): 123748–123757, https://doi.org/10.1016/j.molliq.2023.123748.

32. X. X. Ye, Z. H. Zheng, R. Y. Chi, J. Liu, J. Chen, and W. Luo, "Waste for Waste: Interface-Intensified Durable Superhydrophilic-Superoleophobic Collagen Fiber Membrane for Efficient Separation of Cationic Surfactant-Stabilized Oil-In-Water Emulsions," *Langmuir* 39 (2023): 18815–18824, https://doi.org/10.1021/acs.langmuir.3c02493.

33. X. Y. Zhang, C. Q. Wang, X. Y. Liu, J. Wang, C. Zhang, and Y. Wen, "A Durable and High-Flux Composite Coating Nylon Membrane for Oil-Water Separation," *Journal of Cleaner Production* 193 (2018): 702–708, https://doi.org/10.1016/j.jclepro.2018.05.102.

34. F. U. Ahmed and D. D. Purkayastha, "Superhydrophilic ZnO Nano-Needle Decorated Over Nanofibrous PAN Membrane and its Application Towards Oil/Water Separation," *Journal of Environmental Chemical Engineering* 11 (2023): 111166–111179, https://doi.org/10.1016/j.jece.2023.111166.

35. Y. I. Guo, M. Li, X. Wen, Y. Guo, X. Guo, and T. Zhang, "Silica-Modified Electrospun Membrane With Underwater Superoleophobicity for Effective Gravity-Driven Oil/Water Separation," *Fibers and Polymers* 23, no. 7 (2022): 1906–1914, https://doi.org/10.1007/s12221-022-4039-x.

36. Z. M. Zhang, Z. Q. Gan, R. Y. Bao, et al., "Green and Robust Superhydrophilic Electrospun Stereocomplex Polylactide Membranes: Multifunctional Oil/Water Separation and Self-Cleaning," *Journal of Membrane Science* 593 (2020): 117420–117428, https://doi.org/10.1016/j.memsci.2019.117420.

37. B. Than-Ardna, C. Weder, and H. Manuspiya, "Superhydrophilic Bacterial Cellulose Membranes Efficiently Separate Oil-in-Water Emulsions," *Journal of Materials Science* 58 (2023): 5086–5103, https://doi.org/10.1007/s10853-023-08278-w.

38. J. Usman, N. Baig, and I. H. Aljundi, "Superhydrophilic and Underwater Superoleophobic Ceramic Membranes Grafted by Layered Polydopamine and Polydopamine Encapsulated Silica Particles for Efficient Separation of Oil-in-Water Emulsions," *Journal of Environmental Chemical Engineering* 11 (2023): 110011–110024, https://doi.org/10.1016/j.jece.2023.110011.

39. S. B. Zhang, S. L. Pang, L. Jiang, et al., "Poly(Vinylidene Fluoride) Membrane Design for Efficient Oil-in-Water Emulsion Separation: Integrating Superhydrophilicity, Photocatalysis and Self-Cleaning," *Applied Surface Science* 675 (2024): 160948–160958, https://doi.org/10.1016/j.apsusc.2024.160948.

40. X. Q. Cheng, Z. K. Sun, X. B. Yang, et al., "Construction of Superhydrophilic Hierarchical Polyacrylonitrile Nanofiber Membranes by In Situ Asymmetry Engineering for Unprecedently Ultrafast Oil–Water Emulsion Separation," *Journal of Materials Chemistry A* 8, no. 33 (2020): 16933–16942, https://doi.org/10.1039/d0ta03011b.

41. L. Gao, H. H. Gu, C. X. Wang, et al., "Superhydrophilic and Oil-Resistant SiO_2/PU Fiber Membrane for Oil-in-Water Emulsion Separation Under Gravity," *Fibers and Polymers* 25, no. 5 (2024): 1623–1634, https://doi.org/10.1007/s12221-024-00526-3.

42. Y. Y. Mo, F. Zhang, H. F. Dong, et al., "Ultrasmall $Cu_3(PO_4)_2$ Nanoparticles Reinforced Hydrogel Membrane for Super-Antifouling Oil/Water Emulsion Separation," *ACS Nano* 16, no. 12 (2022): 20786–20795, https://doi.org/10.1021/acsnano.2c07977.

43. Y. Z. Zhu, J. L. Wang, F. Zhang, et al., "Zwitterionic Nanohydrogel Grafted PVDF Membranes With Comprehensive Antifouling Property and Superior Cycle Stability for Oil-in-Water Emulsion Separation," *Advanced Functional Materials* 28, no. 40 (2018): 1804121, https://doi.org/10.1002/adfm.201804121.

44. W. H. Qing, X. H. Li, Y. F. Wu, et al., "In Situ Silica Growth for Superhydrophilic-Underwater Superoleophobic Silica/PVA Nanofibrous Membrane for Gravity-Driven Oil-in-Water Emulsion Separation," *Journal of Membrane Science* 612 (2020): 118476–118483, https://doi.org/10.1016/j.memsci.2020.118476.

45. F. Iñiguez-Franco, R. Auras, K. Dolan, et al., "Chemical Recycling of Poly(Lactic Acid) by Water-Ethanol Solutions," *Polymer Degradation and Stability* 149 (2018): 28–38, https://doi.org/10.1016/j.polymdegradstab.2018.01.016.

46. F. K. Metze, S. Sant, Z. Meng, H. A. Klok, and K. Kaur, "Swelling-Activated, Soft Mechanochemistry in Polymer Materials," *Langmuir* 39 (2023): 3546–3557, https://doi.org/10.1021/acs.langmuir.2c02801.

47. A. L. Pang and H. Ismail, "Effects of Kenaf Loading and 3-Aminopropyltriethoxysilane Coupling Agent on the Properties of Polypropylene/Waste Tire Dust/Kenaf Composites," *Journal of Thermoplastic Composite Materials* 27 (2014): 1607–1619, https://doi.org/10.1177/0892705712475002.

48. C. Zhao, J. K. Miao, M. Y. Sui, X. Liu, and Y. Yu, "Colloidal Characteristics, Drug Encapsulation, and Oil-in-Water Emulsion of Dodecenyl-Modified Alginate," *Journal of Surfactants and Detergents* 22 (2019): 633–639, https://doi.org/10.1002/jsde.12272.

49. C. Maier, A. M. Oechsle, and J. Weiss, "Cross-Linking Oppositely Charged Oil-in-Water Emulsions to Enhance Heteroaggregate Stability," *Colloids and Surfaces B: Biointerfaces* 135 (2015): 525–532, https://doi.org/10.1016/j.colsurfb.2015.08.009.

50. G. H. Gao, H. X. Xu, X. H. Yu, et al., "Multifunctional PVDF Nanofiber Materials for High Efficiency Dual Separation of Emulsions and Unidirectional Water Penetration," *Applied Surface Science* 636 (2023): 157808–157818, https://doi.org/10.1016/j.apsusc.2023.157808.

51. W. F. Zhang, R. X. Qu, X. Y. Li, et al., "A Dual Functional Janus Membrane Combining Superwettability With Electrostatic Force for

Controllable Anionic/Cationic Emulsion Separation and In Situ Surfactant Removal," *Journal of Materials Chemistry A* 7, no. 47 (2019): 27156–27163, https://doi.org/10.1039/c9ta10390b.

52. X. F. You, Y. Liao, M. Tian, X. You, J. W. Chew, and R. Wang, "Engineering Highly Effective Nanofibrous Membranes to Demulsify Surfactant-Stabilized Oil-In-Water Emulsions," *Journal of Membrane Science* 611 (2020): 118398–118408, https://doi.org/10.1016/j.memsci.2020.118398.

53. Y. M. Lin, C. Song, and G. C. Rutledge, "Functionalization of Electrospun Membranes With Polyelectrolytes for Separation of Oil-in-Water Emulsions," *Advanced Materials Interfaces* 6 (2019): 1901285, https://doi.org/10.1002/admi.201901285.

54. X. L. Cai, C. J. Li, Q. Tang, et al., "Assembling Kaolinite Nanotube at Water/Oil Interface for Enhancing Pickering Emulsion Stability," *Applied Clay Science* 172 (2019): 115–122, https://doi.org/10.1016/j.clay.2019.02.021.

55. A. M. Cheong and K. L. Nyam, "Improvement of Physical Stability of Kenaf Seed Oil-in-Water Nanoemulsions by Addition of β-Cyclodextrin to Primary Emulsion Containing Sodium Caseinate and Tween 20," *Journal of Food Engineering* 183 (2016): 24–31, https://doi.org/10.1016/j.jfoodeng.2016.03.012.

56. B. He, Y. J. Ding, J. Q. Wang, et al., "Sustaining Fouling Resistant Membranes: Membrane Fabrication, Characterization and Mechanism Understanding of Demulsification and Fouling-Resistance," *Journal of Membrane Science* 581 (2019): 105–113, https://doi.org/10.1016/j.memsci.2019.03.045.

57. C. L. Chen, L. Chen, S. Chen, et al., "Preparation of Underwater Superoleophobic Membranes via TiO_2 Electrostatic Self-Assembly for Separation of Stratified Oil/Water Mixtures and Emulsions," *Journal of Membrane Science* 602 (2020): 117976–117985, https://doi.org/10.1016/j.memsci.2020.117976.

Supporting Information

Additional supporting information can be found online in the Supporting Information section.